

GEOLOGY

Reconciling evidence of oxidative weathering and atmospheric anoxia on Archean Earth

Aleisha C. Johnson^{1,2*}, Chadlin M. Ostrander^{1,3}, Stephen J. Romaniello⁴, Christopher T. Reinhard⁵, Allison T. Greaney⁶, Timothy W. Lyons⁷, Ariel D. Anbar^{1,8}

Evidence continues to emerge for the production and low-level accumulation of molecular oxygen (O₂) at Earth's surface before the Great Oxidation Event. Quantifying this early O₂ has proven difficult. Here, we use the distribution and isotopic composition of molybdenum in the ancient sedimentary record to quantify Archean Mo cycling, which allows us to calculate lower limits for atmospheric O₂ partial pressures (PO₂) and O₂ production fluxes during the Archean. We consider two end-member scenarios. First, if O₂ was evenly distributed throughout the atmosphere, then PO₂ > 10^{-6.9} present atmospheric level was required for large periods of time during the Archean eon. Alternatively, if O₂ accumulation was instead spatially restricted (e.g., occurring only near the sites of O₂ production), then O₂ production fluxes >0.01 Tmol O₂/year were required. Archean O₂ levels were vanishingly low according to our calculations but substantially above those predicted for an abiotic Earth system.

INTRODUCTION

The evolution of Earth's atmosphere and biosphere was profoundly affected by the rise of molecular oxygen (O₂) at the end of the Archean eon [~2.4 billion years (Ga) ago]. Quantification of this initial rise of O₂ remains elusive (1, 2). Most constraints on the partial pressure of O₂ (PO₂) in the Archean atmosphere are upper limits, such as those derived from mass-independent fractionation of sulfur isotopes (MIF-S) [PO₂ < 10⁻⁶ present atmospheric level (PAL); (3–5)], detrital grains of pyrite and uraninite [PO₂ < 10^{-3.8} PAL; (6–9)], and Fe mobility in paleosols [PO₂ < 10^{-4.7} PAL; (10–13)]. These constraints are highly informative with regard to the timing and tempo of the Great Oxidation Event (GOE), which has been dated at ~2.5 to 2.2 Ga based on when the constraints set by MIF-S and other proxies were exceeded (14–18). However, these constraints are less informative about how much O₂, if any, was produced before the GOE, leading many to conclude that there was no O₂ production at all [i.e., (19)].

In contrast, over the past 20 years, several lines of evidence have been interpreted to reflect low levels of oxidative weathering before the GOE, potentially due to transient small amounts of O₂ [also known as “whiffs” of O₂ or Archean oxidation events (AOEs); (2, 20, 21)]. This evidence includes concentration enrichments and shifts in the isotopic compositions of some redox-sensitive elements in marine shales (e.g., Cr, Mo, Re, Tl, and U) [(2) and references therein]. It is important to emphasize that these lines of evidence signify only surface redox cycling of certain elements and not necessarily oxidation by O₂. However, the combination of multiple lines of evidence, including mass-dependent shifts in redox-sensitive light stable isotopes [e.g., (22–24)], observations from stromatolites [e.g., (25)], and the high organic carbon content of Archean shales [e.g., (1)], makes the case for early O₂ compelling. Nevertheless,

questions remain about the levels of PO₂ needed to account for observed signatures of oxidative weathering and whether they can be reconciled with existing upper limits on Archean PO₂.

Molybdenum (Mo) is a particularly useful proxy to address this question because its geochemical cycling and ocean isotope budget are strongly redox-dependent [summarized in (26)]. In the modern environment, Mo is delivered to the ocean as the soluble molybdate oxyanion (MoO₄²⁻) following the oxidative weathering of crustal sulfides by O₂ (27), with some Mo retained in weathering-resistant detrital phases (28). This MoO₄²⁻ is then removed from the ocean primarily by adsorption to ferromanganese oxide minerals or by removal into highly reducing sedimentary environments rich in hydrogen sulfide (29–31). Because the marine Mo cycle relies on the supply of Mo from O₂-induced weathering of Mo from the crust, as well as the removal of Mo into oxidizing and reducing sediments, sedimentary Mo enrichments and isotope values are powerful tracers of Earth surface redox history [e.g., (32, 33)]. More to this point, Mo enrichments and isotope trends found in multiple sets of late-Archean sedimentary rocks are interpreted as indicating accumulation of low levels of O₂ in Archean weathering and marine environments (34–38).

To explore whether oxidative weathering signatures can be reconciled with observations of an anoxic Archean atmosphere, we used observed Mo enrichments and isotope values in Archean shales to constrain a model of Mo mass balance during weathering and ocean accumulation. Using this approach, we can calculate the minimal Mo flux that needs to be delivered to the oceans. This flux, in turn, can be used to explore the viability of different oxidative weathering scenarios. Here, we explore two end-member scenarios, one in which O₂ was well mixed in the Archean atmosphere, and another in which O₂ was produced and accumulated strictly within localized terrestrial microbial communities in the Archean, with little to no atmospheric mixing. These models are used to establish lower limits on the amount of O₂ present in Archean surface environments.

RESULTS

To calculate constraints on Archean O₂ dynamics, we explore two end-member scenarios in our calculations. First, for the purposes of

Copyright © 2021
The Authors, some
rights reserved;
exclusive licensee
American Association
for the Advancement
of Science. No claim to
original U.S. Government
Works. Distributed
under a Creative
Commons Attribution
License 4.0 (CC BY).

Downloaded from https://www.science.org at University of Chicago on February 21, 2024

¹School of Earth and Space Exploration, Arizona State University, Tempe, AZ, USA.

²Department of Geophysical Sciences, University of Chicago, Chicago, IL, USA.

³Department of Marine Chemistry and Geochemistry, Woods Hole Oceanographic Institution, Woods Hole, MA, USA.

⁴Department of Earth and Planetary Sciences, University of Tennessee—Knoxville, Knoxville, TN, USA.

⁵School of Earth and Atmospheric Sciences, Georgia Institute of Technology, Atlanta, GA, USA.

⁶Oak Ridge National Laboratory, Knoxville, TN, USA.

⁷Department of Earth and Planetary Sciences, University of California, Riverside, Riverside, CA, USA.

⁸School of Molecular Sciences, Arizona State University, Tempe, AZ, USA.

*Corresponding author. Email: acjohnson@uchicago.edu

organizing our thinking on Archean oxidative weathering by O_2 , we assume that O_2 is well mixed in the atmosphere even at very low partial pressures. This assumption allows us to treat PO_2 as a constant boundary condition in our weathering model, allowing us to derive lower limits on the average or equivalent PO_2 responsible for stimulating sulfide weathering and mobilizing Mo. These lower limits on PO_2 can then be compared to existing upper limits to test the viability of our first scenario: that oxidative weathering signatures record changes in global PO_2 .

Perhaps more likely, O_2 was a trace gas during the Archean that was not well distributed in the atmosphere and, instead, existed as short-lived gas plumes and O_2 oases in soils and shallow seas [e.g., (39, 40)]. Potentially, O_2 was so short-lived that PO_2 was negligible beyond the immediate environment where O_2 was produced. To place constraints on the O_2 fluxes produced in these settings, we use the stoichiometry of pyrite oxidation by O_2 to calculate the minimum O_2 flux (Tmol/year) responsible for the Mo input recorded by sedimentary rocks. The minimum O_2 flux in itself is a lower limit on terrestrial O_2 production that can be compared with previous estimates of O_2 production by microbial communities and abiotic sources to explore the viability of such a scenario as the source of oxidative weathering signatures. Below, we examine both end-members.

End-member scenario 1: O_2 as a globally distributed trace gas

Our approach used a Monte Carlo analysis to explore the range of plausible Mo mass balance parameters consistent with the Archean

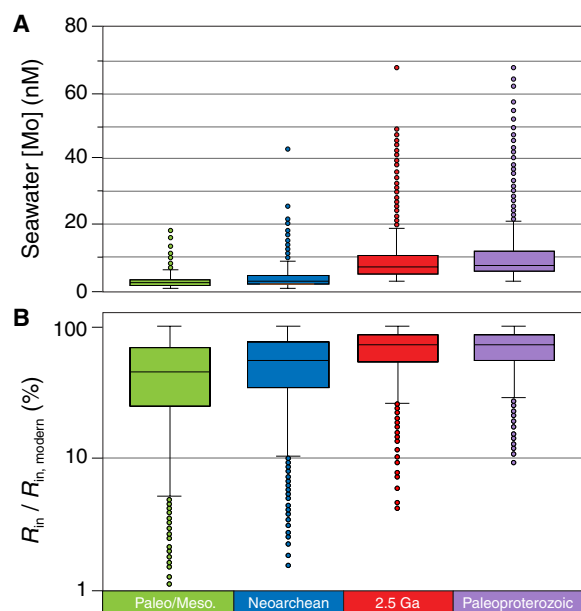


Fig. 1. Requisite seawater [Mo] and Mo input to satisfy mass balance as indicated by ancient shales from 3.2 to 2.0 Ga. (A) Distribution of the seawater Mo concentrations of possible mass balance solutions, where concentrations are reported in $(M \times 10^9)$ (B) Distribution of possible mass balance solutions where Mo input (R_{in}) is plotted as a percentage of the modern riverine Mo flux $[(\text{mol/year})_{\text{MODEL}}] / [(\text{mol/year})_{\text{MODERN}}] \times 100$. Boxes represent the central quartiles of the mass balance solutions (Q2 and Q3) and include a horizontal line to indicate the median. Whiskers represent mass balance solutions that occur within 1.5 quartiles of the boxes; solutions that fall outside this range are plotted as points. Notably, the minimum Mo required of each solution set increases through time.

and Paleoproterozoic shale record (see Materials and Methods). Rather than reconstructing Mo mass balance from the shale record, which has many nonunique solutions, this approach explores all plausible Mo mass balance solutions and selects those that match the shale record. Paired together, Mo isotopic and concentration data are leveraged to place constraints on the total input of Mo required to sustain steady state under different marine redox scenarios. We subdivide the shale record from 3.2 to 2.0 Ga into four periods based on observed Mo concentrations and isotope values: the Paleo/Mesoarchean (3.2 to 2.8 Ga), the Neoarchean (2.8 to >2.5 Ga), the “Whiff of O_2 ” sediments at 2.5 Ga (20), and the Paleoproterozoic (2.5 to 2.0 Ga).

In Fig. 1, we plot the results of the mass balance model: Panel A shows the seawater concentrations of Mo for all plausible mass balance solutions. Panel B shows Mo input to the ocean (R_{in}) from all plausible mass balance solutions, relative to the modern riverine Mo flux. All mass balance solutions from each time period require greater than 1% of the modern Mo flux, meaning they require Mo in excess of potential hydrothermal contributions (see Materials and Methods). By extension of this logic, our model indicates that our estimated hydrothermal contribution would result in Mo enrichments <2 parts per million (ppm), similar to detrital contributions. In both panels of Fig. 1, a distinct trend can be seen: The lower threshold of each mass balance solution set increases approaching and across the Archean-Proterozoic boundary. More specifically, in panel B, the minimum Mo input required to satisfy mass balance increases from ~1% of the modern Mo flux in the Archean to several percent by the end of the Neoarchean and to greater than ~10% in the Paleoproterozoic.

To calculate lower limits on PO_2 , we convert the minimum Mo input (R_{in}) of each time period to PO_2 using a previously published weathering model (Fig. 2). The model used here is that of Daines *et al.* (41), which calculates global sulfate production from oxidative weathering as a function of the rates of continental uplift and

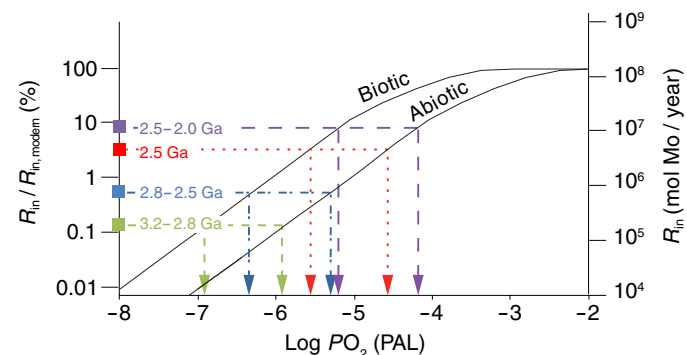


Fig. 2. Calculation of PO_2 requirements. The river flux of Mo that is delivered to the ocean over time is related to PO_2 by calculating R_{in} (mol Mo/year) as the product of sulfide dissolution in global weathering soil profiles (see text and Materials and Methods for description of the weathering model). Modeled trends are included for abiotic sulfide oxidation by O_2 and biotic sulfide oxidation in the presence of O_2 , with the latter considered to be roughly one order of magnitude faster based on biotic sulfide oxidation experiments (43). The minimum Mo requirements of all mass balance solutions for each time period are plotted on these trends, which indicate on the x axis the PO_2 necessary to stimulate oxidative weathering and deliver the necessary flux of Mo to the ocean from crustal sulfides. Because the R_{in} values are minimum requirements for the mass balance solutions, the indicated PO_2 values are similarly minimum estimates.

erosion and PO_2 . Specifically, their study leveraged an existing one-dimensional reaction-transport model and uplift rates from modern river sediment budgets (41). We updated the sulfide oxidation kinetics of the model using the rate law of Johnson *et al.* (42), which specifically determined reaction kinetics at levels of PO_2 relevant to this study ($<10^{-5}$ PAL PO_2). We then multiplied the global sulfate input by the Mo/S ratio of modern rivers (27) as a proxy for the Mo/S ratio of crustal sulfides to calculate the PO_2 -dependent global Mo flux from oxidative weathering of sulfides by O_2 (Fig. 2).

In the modern environment, biology is well known to accelerate mineral sulfide oxidation and is thus important to consider in these weathering calculations. However, because the influence of biology on the weathering rate is not explicitly considered in the model, we include an estimate for biologically mediated sulfide oxidation, which some experiments have identified as being ~ 1 order of magnitude faster than abiotic sulfide oxidation by O_2 [e.g., (43)].

In Fig. 2, we obtain lower limits on PO_2 by comparing the derived Mo input fluxes as a function of PO_2 to our minimum Mo input estimates from each time period, following a correction for potential hydrothermal contribution (see Materials and Methods). From the Paleoproterozoic through the Mesoproterozoic (3.2 to 2.8 Ga), Mo enrichments correspond to a lower limit on PO_2 of $\sim 10^{-6.9}$ PAL. Neoproterozoic enrichments (2.8 to 2.55 Ga) correspond to a lower limit of $PO_2 \geq 10^{-6.3}$ PAL. The enrichments at 2.5 Ga deviate even more substantially from crustal values, requiring $PO_2 \geq 10^{-5.6}$ PAL. Paleoproterozoic enrichments (2.4 to 2.0 Ga) are the largest and contain the most isotopically heavy values, requiring $PO_2 \geq 10^{-5.2}$ PAL.

In Fig. 3, we use the compiled Mo enrichment and isotope values from the shale record to determine over which periods of time we are able to directly place lower limits on PO_2 . We subdivide each era of Archean time into 100-million-year time bins and place lower limits on PO_2 in each interval for which both concentration enrichments and isotope data exist above crustal values. The resulting PO_2 constraints through time thus reflect the temporal spread of available data obtained from the geologic record, which generally decreases further back through time as there are fewer suitable samples. Because Paleo and Mesoproterozoic Mo enrichments are so close to crustal values, we cannot rule out that these earliest Mo “enrichments” were deposited by an anomalous mechanism (i.e., increased Mo sourcing from hydrothermal activity) or that the composition of the upper crust was different at that time relative to our current estimates, leading to false positives for O_2 . However, with our best current assumptions, Mo supply from low-level oxidative weathering remains the most parsimonious explanation for the observed shale enrichments.

The lowest PO_2 estimates presented here are those that consider biologically mediated pyrite oxidation ($PO_2 \geq 10^{-6.9}$ PAL; Figs. 2 and 3C). These estimates are consistent with previously published upper limits on PO_2 , which are ~ 10 times higher (Figs. 2 and 3C). It is thus plausible that the oxidation of crustal sulfide grains was a biologically mediated process for much, if not all, of the Archean [see also (44)]. However, because we also find that the PO_2 required in abiotic scenarios is near existing upper limits, biologically mediated sulfide oxidation may not have been required.

These lower limits for PO_2 agree well with PO_2 upper limits derived from MIF-S, detrital grains, and paleosols (Fig. 3 and Table 1). Together, these constraints could define a plausible Archean O_2 curve that can account for the seemingly paradoxical presence of

oxidative weathering signatures produced under a reducing atmosphere. Similar to the Mo record, these calculated lower limits also increase throughout the Archean, which may imply that O_2 production increased or O_2 sinks decreased during the time leading up to the GOE. These implications are discussed further in later sections.

It may seem counterintuitive that oxidative weathering of sulfides was active in the Archean, given the presence of detrital pyrite grains in many Archean sedimentary successions [e.g., (6, 45, 46)]. As shown in Fig. 2, modeled sulfide oxidation can be subdivided into two regimes: O_2 -limited at low PO_2 and sulfide-limited at high PO_2 . The transition between these two regimes marks a shift in the limiting reactant (O_2 versus pyrite availability) for global sulfide oxidation. In modern highly oxygenated environments, rates of sulfide oxidation are limited by the supply of pyrite and other sulfides in weathering soils, resulting in a zero-order dependence on PO_2 (47). At lower PO_2 , the rate of sulfide oxidation slows to the point where the net rate is limited by O_2 diffusion into weathering soils. Under these latter conditions, the supply of sulfide minerals is not limiting so that detrital pyrite can survive weathering in soils by not fully oxidizing. In the modeling presented here, the transition between these regimes occurs at around 10^{-4} to 10^{-3} PAL, in broad agreement with previous calculations for the oxidation of detrital grains [$PO_2 < 10^{-3.8}$ PAL; (6–9)] and global sulfide weathering models (41, 47). Notably, the time periods examined in this study all fall within the O_2 -limited sulfide oxidation regime.

Consistent with this finding, diamictites from 2.90 to 2.43 Ga show only small degrees of Mo mobilization (48, 49). Retention of Mo in diamictites is also expected because Mo^{4+} often substitutes for Ti^{4+} in titaniferous, weathering-resistant minerals, meaning only a fraction of crustal Mo is hosted in sulfides and mobilized during oxidative weathering (28, 50). For instance, Greaney *et al.* (28) estimated that $\sim 60\%$ of the Mo hosted in the modern upper continental crust could be contained within sulfide minerals. If 1% of sulfide-hosted Mo was liberated due to oxidative weathering, the regolith sampled by diamictites would only record a 0.6% change in total Mo content or less if the diamictites also sampled primary bedrock. In short, the modeling presented here demonstrates that the Mo required to satisfy our mass balance model can be supplied at each stage of the Archean without fully dissolving sulfide minerals, which is consistent with other evidence typically interpreted to support a low- O_2 atmosphere.

End-member scenario 2: O_2 as a nonglobally distributed trace gas

As mentioned previously, it is unlikely that O_2 was well distributed in the atmosphere at levels approaching $\sim 10^{-7}$ PAL PO_2 . To sustain these levels, primary production would have to match or exceed the modern O_2 flux to balance the rapid supply of reduced gases [e.g., (4, 51)]. It is also commonly thought that $\sim 10^{-7}$ PAL PO_2 is a point of atmospheric instability, either resulting in a return to a more reduced state or the oxygenation of the atmosphere [i.e., (52)]. It is much more likely that O_2 was produced locally in soils and shallow seas by microbial communities and rapidly consumed locally by reduced materials before entering the greater atmosphere [e.g., (39, 53, 54)]. In such a scenario, our equivalent PO_2 estimates are still valid as lower limits for the PO_2 experienced by some soils but likely do not reflect the atmosphere in the way that PO_2 inferred from MIF-S does.

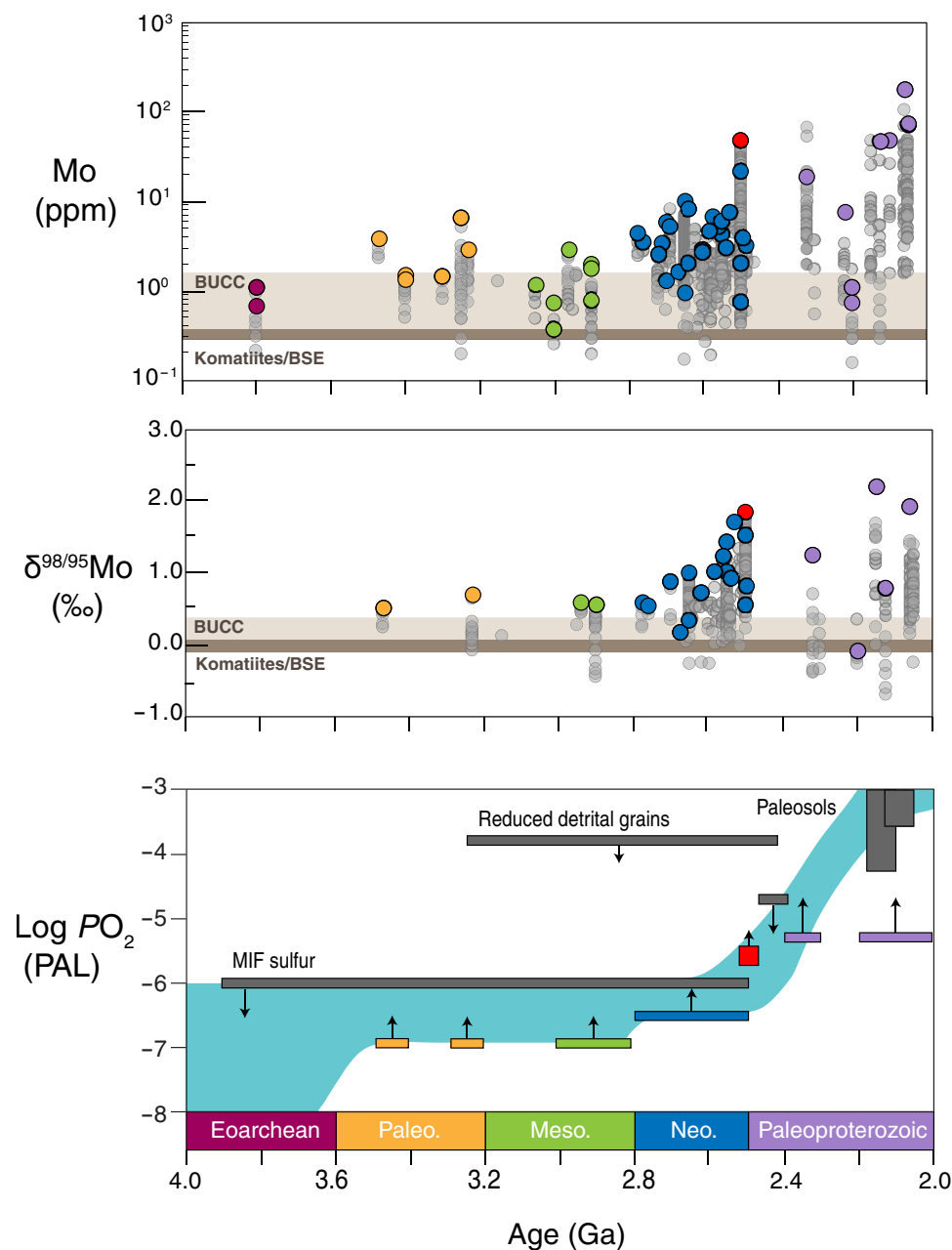
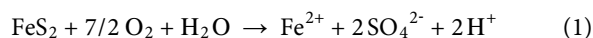


Fig. 3. Archean and Paleoproterozoic estimates of equivalent atmospheric PO_2 derived from Mo concentration enrichments and isotope values in black shales. (A and B) Compiled data for Mo (ppm) and $\delta^{98/95}\text{Mo}$ (‰) in Archean- and Paleoproterozoic-age black shales compared to bulk upper continental crust (BUCC) and values for komatiites and bulk silicate Earth (BSE) (68–70). The maximum value for each particular shale unit is colored, while all other data from each unit are gray (20, 32, 34, 35, 63, 71–84). (C) PO_2 requirements of mass balance solutions that are consistent with Mo concentration enrichments and isotope values in the geologic record, where PO_2 is in units of PAL and compared to previously published PO_2 constraints [5 ($<10^{-6}$ PAL); 6 ($<10^{-3.8}$ PAL before 2.415 Ga); 10 ($<10^{-4.7}$ PAL at ~ 2.46 Ga, $10^{-4.3}$ to $10^{-1.8}$ PAL at ~ 2.15 Ga, $10^{-3.6}$ to $10^{-1.0}$ PAL at ~ 2.08 Ga)].

To evaluate the viability of local O_2 production as the source of oxidative weathering signatures, we can calculate the flux of O_2 implied by Mo and S delivery to the ocean and compare to previous estimates of terrestrial primary productivity. As shown in Fig. 1, all mass balance solutions require some amount of minimum Mo input to the ocean, measured in mol Mo/year. In the previous section, we relate the minimum Mo input from rivers to sulfate input

from sulfide weathering using the Mo/S ratio of modern rivers (27). Using the minimum sulfate input for each time period, we can then use the stoichiometry of pyrite oxidation by O_2 to calculate how many moles of O_2 were consumed by sulfide oxidation, assuming that all oxidizing power was converted to SO_4^{2-} and not Fe^{3+}



This approach indicates that the rate of O_2 consumed by terrestrial sulfide oxidation was on the order of ≥ 0.02 Tmol O_2 /year from 3.5 to 2.8 Ga, increasing to ≥ 0.06 Tmol O_2 /year from 2.8 to 2.55 Ga. At 2.5 Ga, the sudden shift in marine Mo enrichments corresponds to an O_2 flux of ≥ 0.4 Tmol O_2 /year. Paleoproterozoic enrichments require ≥ 1.0 Tmol O_2 /year consumed by terrestrial sulfide oxidation. These estimates are well within the range of proposed O_2 production rates by terrestrial benthic communities, which extend up to 10 Tmol O_2 /year even at 1% or less of modern crustal coverage (53), and are far below modern net primary productivity (~ 10 Tmol O_2 /year) (55). Therefore, local O_2 production by terrestrial microbial communities is a viable mechanism for generating Archean oxidative weathering signatures.

Table 1. Summary of estimates of O_2 levels in the Archean atmosphere.

Archean O_2 estimate	Global or local	Proxy	Minimum or maximum estimate	Author
$PO_2 < 10^{-6}$	Global	MIF-S anomalies	Maximum	(3–5)
$PO_2 < 10^{-3.8}$ PAL	Global	Detrital pyrite and uraninite	Maximum	(6–9)
$PO_2 < 10^{-4.7}$ PAL	Global	Fe mobility in paleosols	Maximum	(10–13)
$PO_2 > 10^{-6.9}$ PAL	Global	Mo in shales	Minimum	This study
> 0.01 Tmol O_2 /year	Local	Mo in shales	Minimum	This study

DISCUSSION

A framework for Archean oxidative weathering

Our study is an example of how new estimates of PO_2 and O_2 production can be derived from existing geochemical data, reconciling observations of Archean oxidative weathering with evidence of a reducing atmosphere. We imagine that O_2 production by terrestrial microbial communities stimulated highly localized oxidative weathering, resulting in the delivery of redox-sensitive trace metals to marine environments (Fig. 4). For most of the Archean, these O_2 sources were greatly exceeded by O_2 sinks and were fairly unimportant in determining atmospheric redox (5, 51). However, the Neoproterozoic observed a substantial rise in O_2 consumption by oxidative weathering of sulfides, primarily surrounding the AOE at 2.5 Ga (20, 21, 44). This pulse of oxidative weathering could have been caused by increased landmass [e.g., (56)], increased O_2 production, or both in the instance where increased landmass promoted terrestrial colonization and the exposure of crustal sulfides to weathering. One could also imagine that if AOE were tied to solid Earth drivers such as landmass, then those same mechanisms may have played a role in triggering the GOE [e.g., (55)]. Future studies leveraging geochemical data to learn about ancient O_2 are well positioned to verify these mechanisms.

At the same time that O_2 was rising in the environment and stimulating sulfide weathering, Mo began accumulating in the oceans at biologically relevant levels. Most of the mass balance solutions from our model indicate that for most of the Archean, seawater concentrations of Mo were below 5 nM (Fig. 1A). This threshold is notable because it was previously identified by culturing experiments to be the limit below which Mo becomes limiting for N_2 fixation in cyanobacteria (57). If Mo was favored as an enzymatic cofactor by this time by N_2 fixers [e.g., (58)], our results imply that periods of biological Mo limitation on N fixation (seawater [Mo] < 5 nM)

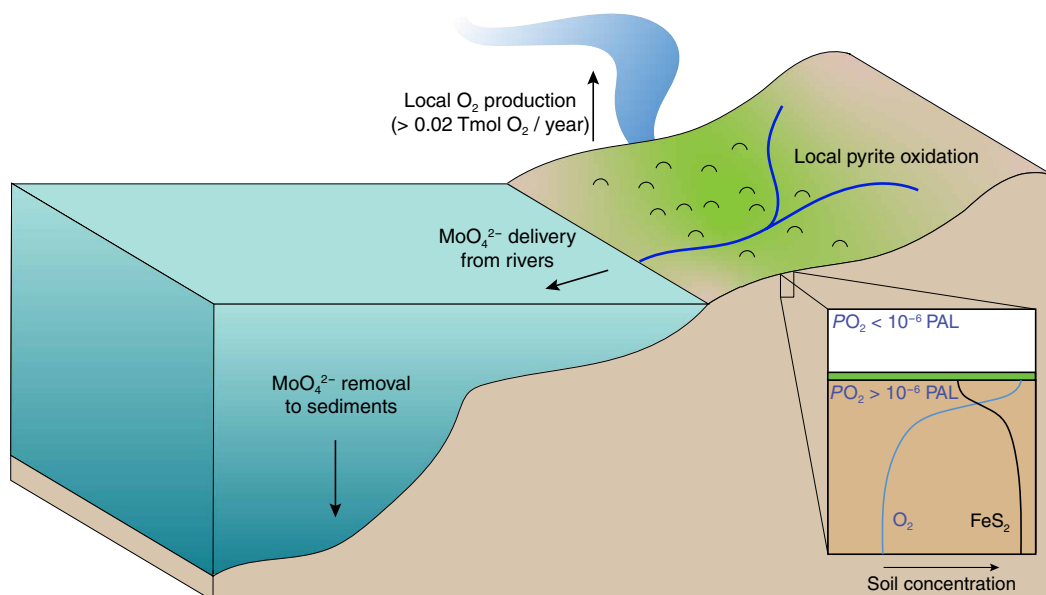


Fig. 4. An emergent view of Archean terrestrial O_2 production. It is likely that oxidative weathering signatures such as Mo enrichments in shales preceded atmospheric oxygenation due to local O_2 production and consumption in terrestrial environments. Shallow soils in proximity to microbial communities (green in the figure) may have experienced greater than $\sim 10^{-7}$ PAL PO_2 , which was capable of partially oxidizing sulfide grains and delivering trace metals such as Mo to rivers and marine environments in excess of hydrothermal or detrital contributions. Until the late Archean, these O_2 fluxes had very little effect on atmospheric redox, which remained $< 10^{-6}$ PAL PO_2 in the presence of rapidly supplied reductants (O_2 sinks).

may have occurred frequently during Archean time, at least on a regional scale (59). Following 2.5 Ga, most mass balance solutions indicate that seawater concentrations of Mo were greater than 5 nM, perhaps ushering in a period where Mo was less likely to be limiting for N₂ fixation in marine environments and representing a potentially important change to the global N cycle. To fully explore this possibility, however, better understanding of large-scale interconnections among Mo availability, biological N fixation and associated thresholds of Mo limitation, contributions from alternative nitrogenase pathways, and the importance of phosphorus (P) limitation is needed. Nevertheless, this feedback may have been important for marine productivity as the rise of O₂ in the marine environment would have promoted loss of fixed N to the atmosphere as N₂ (24, 57, 60).

Last, our study demonstrates that for much of the Archean, the frequent use of “anoxic” should not imply a complete absence of O₂. Low levels of O₂ may have persisted below the MIF-S threshold for hundreds of millions of years before the GOE, with important environmental and biological consequences. More generally, the O₂ lower limits derived here are a first step toward a more nuanced understanding of Archean levels of O₂.

MATERIALS AND METHODS

Monte Carlo analysis

To find viable mass balance solutions to Archean Mo cycling, we use a Monte Carlo model to generate hypothetical data, given a series of source and sink constraints, and use Mo concentration and isotope values from ancient shales to “filter” out implausible results. Our model balances Mo input from rivers and hydrothermal sources against Mo burial in three sedimentary sinks [modified from (26)]: (i) oxide-bearing sediments (Fe oxides, Mn oxides), which are typically deposited beneath oxygenated bottom waters [$>10 \mu\text{M}$ (O₂)]; (ii) sulfidic at depth (SAD) sediments, which are typically deposited beneath suboxic bottom waters and begin to accumulate H₂S in the sediment porewater [$<10 \mu\text{M}$ (O₂), (H₂S) $<11 \mu\text{M}$]; and (iii) euxinic sediments, which are deposited beneath sulfidic bottom waters [$<10 \mu\text{M}$ (O₂), (H₂S) $>11 \mu\text{M}$].

We consider a steady-state mass balance model of Mo concentrations in seawater as a function of Mo inputs and outputs [modified from (61)]. The key governing equations are

$$R_{\text{out},i} = b_i \times [\text{Mo}]_{\text{sw}} \times A_i \quad (2)$$

$$R_{\text{in}} = R_{\text{out}} = \sum R_{\text{out},i} \quad (3)$$

$$f_i = R_{\text{out},i}/R_{\text{out}} \quad (4)$$

$$\delta^{98}\text{Mo}_{\text{in}} = \delta^{98}\text{Mo}_{\text{out}} = \sum (f_i \times \delta^{98}\text{Mo}_i) \quad (5)$$

where $R_{\text{out},i}$ is the rate of Mo removal (mol year⁻¹) to each sedimentary environment i (i.e., oxide-bearing, SAD, or euxinic); b_i is an effective rate constant for removal of Mo (liter km⁻² year⁻¹); $[\text{Mo}]_{\text{sw}}$ is the concentration of Mo in seawater (M); A_i is the depositional area of that sedimentary environment (km²) (where $\cdot A_i$ = total areal extent of the modern seafloor); R_{in} and R_{out} are the total input and output rates of Mo to and from the oceans, respectively (mol year⁻¹); f_i is the fraction of the total Mo output represented by each particular sedimentary environment; and $\delta^{98}\text{Mo}$ (‰) are the isotope

compositions of each sedimentary environment (where $\delta^{98}\text{Mo} = (^{98/95}\text{Mo}_{\text{sample}}/^{98/95}\text{Mo}_{\text{standard}} - 1) \times 1000$).

The isotope compositions are additionally constrained by the relationships $\delta^{98}\text{Mo}_{\text{euxinic}} = \delta^{98}\text{Mo}_{\text{sw}}$, $\delta^{98}\text{Mo}_{\text{oxide}} = \delta^{98}\text{Mo}_{\text{sw}} + \Delta_{\text{sw-oxide}}$, and $\delta^{98}\text{Mo}_{\text{SAD}} = \delta^{98}\text{Mo}_{\text{sw}} + \Delta_{\text{sw-SAD}}$. Here, $\Delta_{\text{sw-}i}$ are respective isotope fractionation factors inferred from field observations and laboratory experiments (Table 2). We assume that $\delta^{98}\text{Mo}_{\text{euxinic}} = \delta^{98}\text{Mo}_{\text{sw}}$ because it is likely that highly reducing sediments at this time could quantitatively remove the small amounts of Mo from overlying seawater. For $\Delta_{\text{sw-oxide}}$, we can subdivide into two sediment types with distinct fractionation behavior: Mn oxide-bearing sediments ($\Delta_{\text{sw-Mn}}$) and Fe oxide-bearing sediments ($\Delta_{\text{sw-Fe}}$). This step is additionally important to account for the possibility of sediments deposited beneath ferruginous [Fe(II)-rich] water columns, which may preserve Fe oxides in the absence of O₂ and H₂S. For Fe oxide-bearing sediments, we select a fractionation factor of 1.25‰, a median value between the fractionation factors of magnetite ($\Delta^{98}\text{Mo} = 0.83 \pm 0.60\text{‰}$), ferrihydrite (ferrihydrite ($\Delta^{98}\text{Mo} = 1.11 \pm 0.15\text{‰}$), goethite ($\Delta^{98}\text{Mo} = 1.40 \pm 0.48\text{‰}$), and hematite ($\Delta^{98}\text{Mo} = 2.19 \pm 0.54\text{‰}$) (62).

The b_i values are calibrated from modern settings and are derived as follows: $R_{\text{out},i} = r_i \times [\text{Mo}]_i \times A_i$, where r_i is the Mo burial rate for sediment i (kg km⁻² year⁻¹), and $[\text{Mo}]_i = a_i \times [\text{Mo}]_{\text{sw}}$, where a_i is a distribution coefficient relating sediment and seawater concentrations (liter kg⁻¹). Hence, $R_{\text{out},i} = r_i \times a_i \times [\text{Mo}]_{\text{sw}} \times A_i = b_i \times [\text{Mo}]_{\text{sw}} \times A_i$, where $b_i = r_i \times a_i$.

Using this framework, $[\text{Mo}]_{\text{sw}}$ can be calculated from derived parameters when combined with key measurements such as $\delta^{98}\text{Mo}_{\text{euxinic}}$ in ancient black shales. However, the derived parameters, particularly A_i and b_i , encompass considerable uncertainties, and the system of equations is underconstrained so that there are many nonunique solutions. There are also uncertainties about overall ocean mass balance because R_{in} is not well constrained.

Table 2. Parameters used in Monte Carlo analysis.

Parameter	Range	References
Depositional area ($A_{\text{D}i}$) (% total)		
Fe oxides	0.01–100	
Mn oxides	0.01–10	(38)
SAD	0.01–100	
Euxinic	0.01–5	(61)
Burial rate constant (b_i) (liter km ⁻² year ⁻¹)		
Fe oxides	1.0–3.0 ($\times 10^6$)	(32)
Mn oxides	1.0–3.0 ($\times 10^6$)	(32)
SAD	1.75–4.25 ($\times 10^8$)	(32)
Euxinic	0.6–1.8 ($\times 10^9$)	(32)
Fractionation factor ($\Delta_{\text{sw-}i}$) (‰)		
Fe oxides	1.25	(62)
Mn oxides	3	(85)
SAD	0.7	(26)
Euxinic	0	(26)
Seawater Mo ($[\text{Mo}]_{\text{sw}}$) (M)	0.01–105 ($\times 10^{-9}$)	
River $\delta^{98/95}\text{Mo}$ ($\delta^{98/95}\text{Mo}_{\text{in}}$) (‰ _{0in})	0–0.7	(26)

To explore this parameter space, we use a Monte Carlo analysis whereby b_i , $[\text{Mo}]_{\text{sw}}$, $\delta^{98}\text{Mo}_{\text{in}}$, and A_i are varied, assuming either a uniform probability distribution or a normal probability distribution across all plausible ranges (Table 2). For instance, $[\text{Mo}]_{\text{sw}}$ is varied from extremely low concentrations (0.01×10^{-9} M) to modern marine concentrations (105×10^{-9} M) using a uniform probability distribution that reflects our lack of constraints on ancient seawater $[\text{Mo}]$. For compositions of sediment that had a low likelihood of extending beyond continental margins (euxinic and Mn oxide-bearing sediments), we limit A_D ranges to $<5\%$ and $<10\%$ of the total ocean floor, respectively. Because the deep ocean was likely ferruginous and may have contained SAD sediments or Fe oxide-bearing sediments, depending on S availability, we explore the full range of depositional area for these sediment compositions. Burial rate constants (b) were sampled using a normal distribution because they are measured values. For b value ranges, uncertainty was set at $\sim\pm 25\%$ of the measured modern value to represent not only analytical uncertainty but also uncertainty with respect to how these values apply to Archean marine sediments. This analysis produces several million solutions to the mass balance equations, which we then filter using constraints from the modern environment and geologic record to eliminate implausible results.

For modeling purposes, the Archean is subdivided into two categories based on geologic eras of distinct shale-hosted Mo enrichment concentrations and isotopic values: the Paleo and Mesoarchean, and the Neoproterozoic. The whiff of O_2 at 2.5 Ga comprises a third category due to its anomalous nature and is not included with other Neoproterozoic sediments. For comparative purposes, we also include a fourth category for the Paleoproterozoic. Compiled data can be found in the Supplementary Materials.

Filtering mass balance solutions

Filtering of mass balance solutions for each time period varied according to available constraints (Table 3). The first filter removed all scenarios that required a greater flux of Mo to the ocean than that which is observed in the modern environment (Table 3). The reasoning behind this constraint is that in the modern highly oxygenated environment, crustal sulfides dissolve completely, and thus, Mo delivery from oxidative weathering is maximized. At lower concentrations of atmospheric O_2 , we assume that crustal Mo delivery could only be less than the modern.

The second filter removed all scenarios that did not produce an isotopic composition in euxinic sediments within the heaviest range typically observed for a given time period (Table 3). We assumed that ancient euxinic sediments captured $\delta^{98/95}\text{Mo}_{\text{SW}}$ values at the time of deposition [although this is not always the case; see Kendall *et al.* (26) and references therein], which allowed the second filter to remove model solutions that produced $\delta^{98}\text{Mo}_{\text{SW}}$ values outside the analytical uncertainty of the heaviest shale $\delta^{98/95}\text{Mo}$ values. The reasoning here is that the Mo contained within shales is a mix of detritally hosted Mo and authigenic Mo, meaning that the $\delta^{98/95}\text{Mo}$ values of these shales are always equal to or lighter than contemporaneous $\delta^{98/95}\text{Mo}_{\text{SW}}$ (63). The heaviest values of $\delta^{98/95}\text{Mo}$ in Archean euxinic shales are thus those with the least crustal influence and are the most likely to have captured ancient $\delta^{98/95}\text{Mo}_{\text{SW}}$.

A third filter removed scenarios where the depositional area of euxinic sediments exceeded the depositional area of SAD sediments. This logic has been applied before to Mo mass balance solutions [i.e., (64)] to avoid unrealistic scenarios where hypothetical euxinic

Table 3. Parameters used for filtering.

Parameter	Range	References
Seawater $\delta^{98/95}\text{Mo}$ (‰)		See compiled data sources
Paleo-Mesoarchean	0.45–0.75	
Neoproterozoic	0.90–1.20	
Whiff (2.5 Ga)	1.50–1.80	
Paleoproterozoic	1.30–2.00	
Maximum shale Mo enrichment ($\mu\text{g g}^{-1}$)		See compiled data sources
Paleo-Mesoarchean	2–5	
Neoproterozoic	5–10	
Whiff (2.5 Ga)	35–50	
Paleoproterozoic	40–70	
Maximum shale sedimentary rate ($\text{g cm}^{-2}\text{ year}^{-1}$)	0.0125	(61)
Minimum shale sedimentary rate ($\text{g cm}^{-2}\text{ year}^{-1}$)	0.00125	(61)
Modern river Mo flux (F_{in}) (mol year^{-1})	1.35×10^8	

sediments coexist with oxide-bearing sediments and lack the SAD sediments that would exist in the transition between. We expect that the formation of euxinic and SAD sediments scales together; thus, in all of our final mass balance solutions, $A_{\text{DSAD}} > A_{\text{DE}}$.

Last, a fourth filter removed all scenarios that did not reproduce the concentrations of Mo within the range observed in ancient euxinic shales (Table 3). For each condition, the flux of Mo to euxinic sediments is divided by a maximum and minimum mass accumulation rate to calculate the range of possible authigenic enrichments. If a mass balance solution produced both a minimum and maximum enrichment that were outside the range observed in shales, it was removed. All ranges in Table 3 capture the maximum enrichments observed in black shales during a given time period, including variability between similarly aged rock units. The lower cutoff is $2 \mu\text{g g}^{-1}$ because enrichments <2 may simply reflect Mo in detrital grains. The range of sedimentation rates was modified from those used by Reinhard *et al.* (61), which were derived from the sedimentation rates of modern anoxic/euxinic basins connected to the open ocean (e.g., Cariaco basin). Here, we vary sedimentation rate by an order of magnitude to ensure that all potentially realistic scenarios are captured by the modeling.

Hydrothermal input

With the lower limits on Mo input to the ocean from Fig. 1, it is now possible to place constraints on oxidative weathering and, by extension, PO_2 . First, we subtract the potential hydrothermal Mo input to prevent overestimating Mo input from oxidative weathering. Where data have been collected in the modern environment, it appears that both high-temperature and low-temperature fluid alterations of the lithosphere can result in Mo-bearing fluids (27, 65, 66). Low-temperature fluids are an important source of Mo to the modern ocean, on the order of 13% of Mo input from rivers (27). However, there is evidence that suggests that the Mo in low-temperature

fluids is sourced from the reductive dissolution of Mo-bearing sediments overlying oceanic crust (67), and thus, low-temperature fluids more closely represent a failed Mo sink rather than a Mo source over geologic time scales. High-temperature fluids were once estimated to contribute 1% of the Mo input from rivers (27, 65), although they are now established to be a net sink in the modern environment (27). It is not yet clear whether the Mo released from high-temperature vents is inherited from seawater or from leaching of the basalt, which makes it difficult to extrapolate to Archean oceans. If Mo is readily leached from basalt during high-temperature alteration, hydrothermal activity could have been an important anoxic source of Mo to Archean seawater. Consequently, our R_{in} values would overestimate the role of oxidative weathering in supplying Mo to the ocean.

To account for the possibility that Archean hydrothermal sources of Mo were important, we subtract 1% of the modern Mo input from our R_{in} values to estimate the contribution of hydrothermal sources, based on the values of Wheat *et al.* (66). This approach more accurately calculates the minimum Mo input from oxidative weathering. Following this correction, we selected the lowest Mo flux for PO_2 and O_2 flux calculations.

SUPPLEMENTARY MATERIALS

Supplementary material for this article is available at <https://science.org/doi/10.1126/sciadv.abj0108>

REFERENCES AND NOTES

1. T. W. Lyons, C. T. Reinhard, N. J. Planavsky, The rise of oxygen in Earth's early ocean and atmosphere. *Nature* **506**, 307–315 (2014).
2. C. M. Ostrander, A. C. Johnson, A. D. Anbar, Earth's first redox revolution. *Annu. Rev. Earth Planet. Sci.* **49**, 337–366 (2021).
3. A. A. Pavlov, J. F. Kasting, Mass-independent fractionation of sulfur isotopes in Archean sediments: Strong evidence for an anoxic Archean atmosphere. *Astrobiology* **2**, 27–41 (2002).
4. K. Zahnle, M. Claire, D. Catling, The loss of mass-independent fractionation in sulfur due to a Palaeoproterozoic collapse of atmospheric methane. *Geobiology* **4**, 271–283 (2006).
5. D. C. Catling, K. J. Zahnle, The Archean atmosphere. *Sci. Adv.* **6**, eaax1420 (2020).
6. J. E. Johnson, A. Gerpheide, M. P. Lamb, W. W. Fischer, O_2 constraints from Paleoproterozoic detrital pyrite and uraninite. *GSA Bull.* **126**, 813–830 (2014).
7. D. E. Grandstaff, Origin of uraniferous conglomerates at Elliot Lake, Canada and Witwatersrand, South Africa: Implications for oxygen in the Precambrian atmosphere. *Precambrian Res.* **13**, 1–26 (1980).
8. H. E. Frimmel, Archean atmospheric evolution: Evidence from the Witwatersrand gold fields, South Africa. *Earth Sci. Rev.* **70**, 1–46 (2005).
9. C. T. Reinhard, R. Raiswell, C. Scott, A. D. Anbar, T. W. Lyons, A late Archean sulfidic sea stimulated by early oxidative weathering of the continents. *Science* **326**, 713–716 (2009).
10. Y. Kanzaki, T. Murakami, Estimates of atmospheric O_2 in the Paleoproterozoic from paleosols. *Geochim. Cosmochim. Acta* **174**, 263–290 (2016).
11. T. Murakami, B. Sreenivas, S. D. Sharma, H. Sugimori, Quantification of atmospheric oxygen levels during the Paleoproterozoic using paleosol compositions and iron oxidation kinetics. *Geochim. Cosmochim. Acta* **75**, 3982–4004 (2011).
12. W. Yang, H. D. Holland, The Heekpoort paleosol profile in Strata 1 at Gaborone, Botswana: Soil formation during the Great Oxidation Event. *Am. J. Sci.* **303**, 187–220 (2003).
13. R. Rye, H. D. Holland, Paleosols and the evolution of atmospheric oxygen: A critical review. *Am. J. Sci.* **298**, 621–672 (1998).
14. G. Luo, S. Ono, N. J. Beukes, D. T. Wang, S. Xie, R. E. Summons, Rapid oxygenation of Earth's atmosphere 2.33 billion years ago. *Sci. Adv.* **2**, 1600134 (2016).
15. A. P. Gumsley, K. R. Chamberlain, W. Bleeker, U. Söderlund, M. O. de Kock, E. R. Larsson, A. Bekker, Timing and tempo of the Great Oxidation Event. *Proc. Natl. Acad. Sci. U.S.A.* **114**, 1811–1816 (2017).
16. P. Philippot, J. N. Ávila, B. A. Killingsworth, S. Tessalina, F. Baton, T. Caqueneau, E. Muller, E. Pecoits, P. Cartigny, S. V. Lalonde, T. R. Ireland, C. Thomazo, M. J. van Kranendonk, V. Busigny, Globally asynchronous sulphur isotope signals require re-definition of the Great Oxidation Event. *Nat. Commun.* **9**, 2245 (2018).
17. M. R. Warke, T. Di Rocco, A. L. Zerkle, A. Lepland, A. R. Prave, A. P. Martin, Y. Ueno, D. J. Condon, M. W. Claire, The Great Oxidation Event preceded a Paleoproterozoic "snowball Earth". *Proc. Natl. Acad. Sci. U.S.A.* **117**, 13314–13320 (2020).
18. S. W. Poulton, A. Bekker, V. M. Cumming, A. L. Zerkle, D. E. Canfield, D. T. Johnston, A 200-million-year delay in permanent atmospheric oxygenation. *Nature* **592**, 232–236 (2021).
19. W. W. Fischer, J. Hemp, J. E. Johnson, Evolution of oxygenic photosynthesis. *Annu. Rev. Earth Planet. Sci.* **44**, 647–683 (2016).
20. A. D. Anbar, Y. Duan, T. W. Lyons, G. L. Arnold, B. Kendall, R. A. Creaser, A. J. Kaufman, G. W. Gordon, C. Scott, J. Garvin, R. Buick, A whiff of oxygen before the great oxidation event? *Science* **317**, 1903–1906 (2007).
21. M. C. Koehler, R. Buick, M. A. Kipp, E. E. Stüeken, J. Zaloumis, Transient surface ocean oxygenation recorded in the ~2.66-Ga Jeerinah Formation, Australia. *Proc. Natl. Acad. Sci. U.S.A.* **115**, 7711–7716 (2018).
22. A. J. Kaufman, D. T. Johnston, J. Farquhar, A. L. Masterson, T. W. Lyons, S. Bates, A. D. Anbar, G. L. Arnold, J. Garvin, R. Buick, Late Archean biospheric oxygenation and atmospheric evolution. *Science* **317**, 1900–1903 (2007).
23. J. Garvin, R. Buick, A. D. Anbar, G. L. Arnold, A. J. Kaufman, Isotopic evidence for an aerobic nitrogen cycle in the latest Archean. *Science* **323**, 1045–1048 (2009).
24. L. V. Godfrey, P. G. Falkowski, The cycling and redox state of nitrogen in the Archean ocean. *Nat. Geosci.* **2**, 725–729 (2009).
25. T. Bosak, A. H. Knoll, A. P. Petroff, The meaning of stromatolites. *Annu. Rev. Earth Planet. Sci.* **41**, 21–44 (2013).
26. B. Kendall, T. W. Dahl, A. D. Anbar, The stable isotope geochemistry of molybdenum. *Rev. Mineral. Geochem.* **82**, 683–732 (2017).
27. C. A. Miller, B. Peucker-Ehrenbrink, B. D. Walker, F. Marcantonio, Re-assessing the surface cycling of molybdenum and rhenium. *Geochim. Cosmochim. Acta* **75**, 7146–7179 (2011).
28. A. T. Greaney, R. L. Rudnick, R. M. Gaschnig, J. B. Whalen, B. Luais, J. D. Clemens, Geochemistry of molybdenum in the continental crust. *Geochim. Cosmochim. Acta* **238**, 36–54 (2018).
29. B. E. Erickson, G. R. Helz, Molybdenum(VI) speciation in sulfidic waters: Stability and lability of thiomolybdates. *Geochim. Cosmochim. Acta* **64**, 1149–1158 (2000).
30. B. C. Bostick, S. Fendorf, G. R. Helz, Differential adsorption of molybdate and tetrathiomolybdate on pyrite (FeS₂). *Environ. Sci. Technol.* **37**, 285–291 (2003).
31. G. R. Helz, E. Bura-Nakić, N. Mikac, I. Ciglencečki, New model for molybdenum behavior in euxinic waters. *Chem. Geol.* **284**, 323–332 (2011).
32. C. Scott, T. W. Lyons, A. Bekker, Y. A. Shen, S. W. Poulton, X. L. Chu, A. D. Anbar, Tracing the stepwise oxygenation of the Proterozoic ocean. *Nature* **452**, 456–459 (2008).
33. C. Scott, T. W. Lyons, Contrasting molybdenum cycling and isotopic properties in euxinic versus non-euxinic sediments and sedimentary rocks: Refining the paleoproxies. *Chem. Geol.* **324–325**, 19–27 (2012).
34. C. Siebert, J. D. Kramers, T. Meisel, P. Morel, T. F. Nägler, PGE, Re-Os, and Mo isotope systematics in Archean and early Proterozoic sedimentary systems as proxies for redox conditions of the early Earth. *Geochim. Cosmochim. Acta* **69**, 1787–1801 (2005).
35. M. Wille, J. D. Kramers, T. F. Nägler, N. J. Beukes, S. Schröder, T. Meisel, J. P. Lacassie, M. Voegelin, Evidence for a gradual rise of oxygen between 2.6 and 2.5 Ga from Mo isotopes and Re-PGE signatures in shales. *Geochim. Cosmochim. Acta* **71**, 2417–2435 (2007).
36. Y. Duan, A. D. Anbar, G. L. Arnold, T. W. Lyons, G. W. Gordon, B. Kendall, Molybdenum isotope evidence for mild environmental oxygenation before the Great Oxidation Event. *Geochim. Cosmochim. Acta* **74**, 6655–6668 (2010).
37. A. R. Cabral, R. A. Creaser, T. Nägler, B. Lehmann, A. R. Voegelin, B. Belyatsky, J. Pašava, A. S. Gomes Jr., H. Galbiatti, M. E. Böttcher, P. Escher, Trace-element and multi-isotope geochemistry of Late-Archean black shales in the Carajás iron-ore district, Brazil. *Chem. Geol.* **362**, 91–104 (2013).
38. C. M. Ostrander, S. G. Nielsen, J. D. Owens, B. Kendall, G. W. Gordon, S. J. Romaniello, A. D. Anbar, Fully oxygenated water columns over continental shelves before the Great Oxidation Event. *Nat. Geosci.* **12**, 186–191 (2019).
39. S. L. Olson, L. R. Kump, J. F. Kasting, Quantifying the areal extent and dissolved oxygen concentrations of Archean oxygen oases. *Chem. Geol.* **362**, 35–43 (2013).
40. P. Liu, C. E. Harman, J. F. Kasting, Y. Hu, J. Wang, Can organic haze and O_2 plumes explain patterns of sulfur mass-independent fractionation during the Archean? *Earth Planet. Sci. Lett.* **526**, 115767 (2019).
41. S. J. Daines, B. J. Mills, T. M. Lenton, Atmospheric oxygen regulation at low Proterozoic levels by incomplete oxidative weathering of sedimentary organic carbon. *Nat. Commun.* **8**, 14379 (2017).
42. A. C. Johnson, S. J. Romaniello, C. T. Reinhard, D. D. Gregory, E. Garcia-Robledo, N. P. Revsbech, D. E. Canfield, T. W. Lyons, A. D. Anbar, Experimental determination of pyrite and molybdenite oxidation kinetics at nanomolar oxygen concentrations. *Geochim. Cosmochim. Acta* **249**, 160–172 (2019).
43. M. Gleisner, R. B. Herbert Jr., P. C. F. Kockum, Pyrite oxidation by *Acidithiobacillus ferrooxidans* at various concentrations of dissolved oxygen. *Chem. Geol.* **225**, 16–29 (2006).
44. E. E. Stüeken, D. C. Catling, R. Buick, Contributions to late Archean sulphur cycling by life on land. *Nat. Geosci.* **5**, 722–725 (2012).
45. H. D. Holland, Model for the evolution of the Earth's atmosphere, in *Petrologic Studies: A Volume to Honor A. F. Buddington*, A. E. J. Engel, H. L. James, B. F. Leonard, Eds. (Geological Society America, 1962), pp. 447–477.

46. B. Rasmussen, R. Buick, Redox state of the Archean atmosphere: Evidence from detrital heavy minerals in ca. 3250–2750 Ma sandstones from the Pilbara Craton, Australia. *Geology* **27**, 115–118 (1999).
47. X. Gu, P. J. Heaney, F. D. A. Aarão Reis, S. L. Brantley, Deep abiotic weathering of pyrite. *Science* **370**, eabb8092 (2020).
48. R. M. Gaschnig, R. L. Rudnick, W. F. McDonough, A. J. Kaufman, Z. Hu, S. Gao, Onset of oxidative weathering of continents recorded in the geochemistry of ancient glacial diamictites. *Earth Planet. Sci. Lett.* **408**, 87–99 (2014).
49. A. T. Greaney, R. L. Rudnick, S. J. Romaniello, A. C. Johnson, R. M. Gaschnig, A. D. Anbar, Molybdenum isotope fractionation in glacial diamictites tracks the onset of oxidative weathering of the continental crust. *Earth Planet. Sci. Lett.* **534**, 116083 (2020).
50. S. Li, W. D. Junkin, R. M. Gaschnig, R. D. Ash, P. M. Piccoli, P. A. Candelà, R. L. Rudnick, Molybdenum contents of sulfides in ancient glacial diamictites: Implications for molybdenum delivery to the oceans prior to the Great Oxidation Event. *Geochim. Cosmochim. Acta* **278**, 30–50 (2020).
51. J. Hao, D. A. Sverjensky, R. M. Hazen, Redox states of Archean surficial environments: The importance of H₂g instead of O₂g for weathering reactions. *Chem. Geol.* **521**, 49–58 (2019).
52. B. S. Gregory, M. W. Claire, S. Rugheimer, Photochemical modelling of atmospheric oxygen levels confirms two stable states. *Earth Planet. Sci. Lett.* **561**, 116818 (2021).
53. S. V. Lalonde, K. O. Konhauser, Benthic perspective on Earth's oldest evidence for oxygenic photosynthesis. *Proc. Natl. Acad. Sci. U.S.A.* **112**, 995–1000 (2015).
54. N. J. Planavsky, S. A. Crowe, M. Fakhraee, B. Beaty, C. T. Reinhard, B. J. Mills, C. Holstege, K. O. Konhauser, Evolution of the structure and impact of Earth's biosphere. *Nat. Rev. Earth Environ.* **2**, 123–139 (2021).
55. H. D. Holland, Volcanic gases, black smokers, and the Great Oxidation Event. *Geochim. Cosmochim. Acta* **66**, 3811–3826 (2002).
56. J. Hao, A. H. Knoll, F. Huang, R. M. Hazen, I. Daniel, Cycling phosphorus on the Archean Earth: Part I. Continental weathering and riverine transport of phosphorus. *Geochim. Cosmochim. Acta* **273**, 70–84 (2020).
57. A. L. Zerkle, C. H. House, R. P. Cox, D. E. Canfield, Metal limitation of cyanobacterial N₂ fixation and implications for the Precambrian nitrogen cycle. *Geobiology* **4**, 285–297 (2006).
58. E. E. Stüeken, R. Buick, B. M. Guy, M. C. Koehler, Isotopic evidence for biological nitrogen fixation by molybdenum-nitrogenase from 3.2 Gyr. *Nature* **520**, 666–669 (2015).
59. A. D. Anbar, A. H. Knoll, Proterozoic ocean chemistry and evolution: A bioinorganic bridge? *Science* **297**, 1137–1142 (2002).
60. E. E. Stüeken, M. A. Kipp, M. C. Koehler, R. Buick, The evolution of Earth's biogeochemical nitrogen cycle. *Earth Sci. Rev.* **160**, 220–239 (2016).
61. C. T. Reinhard, N. J. Planavsky, L. J. Robbins, C. A. Partin, B. C. Gill, S. V. Lalonde, A. Bekker, K. O. Konhauser, T. W. Lyons, Proterozoic ocean redox and biogeochemical stasis. *Proc. Natl. Acad. Sci. U.S.A.* **110**, 5357–5362 (2013).
62. T. Goldberg, C. Archer, D. Vance, S. W. Poulton, Mo isotope fractionation during adsorption to Fe (oxyhydr)oxides. *Geochim. Cosmochim. Acta* **73**, 6502–6516 (2009).
63. C. M. Ostrander, B. Kendall, S. L. Olson, T. W. Lyons, G. W. Gordon, S. J. Romaniello, W. Zheng, C. T. Reinhard, M. Roy, A. D. Anbar, An expanded shale δ⁹⁸Mo record permits recurrent shallow marine oxygenation during the Neoproterozoic. *Chem. Geol.* **532**, 119391 (2020).
64. B. Kendall, G. W. Gordon, S. W. Poulton, A. D. Anbar, Molybdenum isotope constraints on the extent of late Paleoproterozoic ocean euxinia. *Earth Planet. Sci. Lett.* **307**, 450–460 (2011).
65. S. Metz, J. H. Trefry, Chemical and mineralogical influences on concentrations of trace metals in hydrothermal fluids. *Geochim. Cosmochim. Acta* **64**, 2267–2279 (2000).
66. C. G. Wheat, M. J. Mottl, M. Rudnicki, Trace element and REE composition of a low-temperature ridge-flank hydrothermal spring. *Geochim. Cosmochim. Acta* **66**, 3693–3705 (2002).
67. J. McManus, T. Nägler, C. Siebert, C. G. Wheat, D. E. Hammond, Oceanic molybdenum isotope fractionation: Diagenesis and hydrothermal ridge-flank alteration. *Geochem. Geophys. Geosyst.* **3**, 1078 (2002).
68. R. L. Rudnick, S. Gao, Composition of the continental crust, in *Treatise on Geochemistry*, R. L. Rudnick, Ed. (Elsevier, 2003), vol. 3, pp. 1–64.
69. N. D. Greber, I. S. Puchtel, T. F. Nägler, K. Mezger, Komatiites constrain molybdenum isotope composition of the Earth's mantle. *Earth Planet. Sci. Lett.* **421**, 129–138 (2015).
70. M. Willbold, T. Elliott, Molybdenum isotope variations in magmatic rocks. *Chem. Geol.* **449**, 253–268 (2017).
71. C. Alibert, M. T. McCulloch, Rare earth element and neodymium isotopic compositions of the banded iron-formations and associated shales from Hamersley, western Australia. *Geochim. Cosmochim. Acta* **57**, 187–204 (1993).
72. D. Asael, F. L. H. Tissot, C. T. Reinhard, O. Rouxel, N. Dauphas, T. W. Lyons, E. Ponzevera, C. Liorzou, S. Chéron, Coupled molybdenum, iron and uranium stable isotopes as oceanic paleoredox proxies during the Paleoproterozoic Shunga Event. *Chem. Geol.* **362**, 193–210 (2013).
73. D. Asael, O. Rouxel, S. W. Poulton, T. W. Lyons, A. Bekker, Molybdenum record from black shales indicates oscillating atmospheric oxygen levels in the early Paleoproterozoic. *Am. J. Sci.* **318**, 275–299 (2018).
74. S. Eroglu, R. Schoenberg, M. Wille, N. Beukes, H. Taubald, Geochemical stratigraphy, sedimentology, and Mo isotope systematics of the ca. 2.58–2.50 Ga-old Transvaal Supergroup carbonate platform, South Africa. *Precambrian Res.* **266**, 27–46 (2015).
75. B. Kendall, C. T. Reinhard, T. W. Lyons, A. J. Kaufman, S. W. Poulton, A. D. Anbar, Pervasive oxygenation along late Archean ocean margins. *Nat. Geosci.* **3**, 647–652 (2010).
76. F. Kurzweil, M. Wille, R. Schoenberg, H. Taubald, M. J. Van Kranendonk, Continuously increasing δ⁹⁸Mo values in Neoproterozoic black shales and iron formations from the Hamersley Basin. *Geochim. Cosmochim. Acta* **164**, 523–542 (2015).
77. C. Manikyamba, R. Kerrich, Geochemistry of black shales from the Neoproterozoic Sandur Superterrane, India: First cycle volcanogenic sedimentary rocks in an intraoceanic arc-trench complex. *Geochim. Cosmochim. Acta* **70**, 4663–4679 (2006).
78. S. M. McLennan, S. R. Taylor, K. A. Eriksson, Geochemistry of Archean shales from the Pilbara Supergroup, Western Australia. *Geochim. Cosmochim. Acta* **47**, 1211–1222 (1983).
79. S. M. McLennan, S. R. Taylor, T. A. Kröner, Geochemical evolution of Archean shales from South Africa. I. The Swaziland and Pongola Supergroups. *Precambrian Res.* **22**, 91–124 (1983b).
80. S. M. McLennan, S. R. Taylor, V. R. McGregor, Geochemistry of Archean metasedimentary rocks from West Greenland. *Geochim. Cosmochim. Acta* **48**, 1–13 (1984).
81. F. O. Ossa, A. Hofmann, M. Wille, J. E. Spangenberg, A. Bekker, S. W. Poulton, B. Eickmann, R. Schoenberg, Aerobic iron and manganese cycling in a redox-stratified Mesoproterozoic epicontinental sea. *Earth Planet. Sci. Lett.* **500**, 28–40 (2018).
82. B. F. F. Reczko, “The geochemistry of the sedimentary rocks of the Pretoria Group, Transvaal sequence,” thesis, University of Pretoria (1996).
83. S. K. Sahoo, N. J. Planavsky, B. Kendall, X. Wang, X. Shi, C. Scott, A. D. Anbar, T. W. Lyons, G. Jiang, Ocean oxygenation in the wake of the Marinoan glaciation. *Nature* **489**, 546–549 (2012).
84. K. E. Yamaguchi, Geochemistry of Archean–Paleoproterozoic black shales: The early evolution of the atmosphere, oceans, and biosphere, thesis, Pennsylvania State University, State College (2002).
85. L. E. Wasylenki, B. A. Rolfe, C. L. Weeks, T. G. Spiro, A. D. Anbar, Experimental investigation of the effects of temperature and ionic strength on Mo isotope fractionation during adsorption to manganese oxides. *Geochim. Cosmochim. Acta* **72**, 5997–6005 (2008).
86. M. Wille, O. Nebel, M. J. Van Kranendonk, R. Schoenberg, I. C. Kleinhans, M. J. Ellwood, Mo–Cr isotope evidence for a reducing Archean atmosphere in 3.46–2.76 Ga black shales from the Pilbara, Western Australia. *Chem. Geol.* **340**, 68–76 (2013).

Acknowledgments: This manuscript was greatly improved by conversations with D. Sumner and M. Claire, editorial handling by S. Naeem, and reviews by E. Stüeken and two anonymous reviewers. **Funding:** We would like to thank our funding sources, including FESD “Dynamics of Earth System Oxygenation” (NSF EAR 1338810 to A.D.A.), NASA Earth and Space Science Fellowship awarded to A.C.J. (80NSSC17K0498), NSF EAR PF to A.C.J. (1952809), and WHOI Postdoctoral Fellowship to C.M.O. C.T.R. acknowledges support from the NASA Astrobiology Institute. We also acknowledge support from the Metal Utilization and Selection across Eons (MUSE) Interdisciplinary Consortium for Astrobiology Research, sponsored by the National Aeronautics and Space Administration Science Mission Directorate (19-ICAR19_2-0007). **Author contributions:** A.D.A. and T.W.L. developed the project idea, and A.C.J., S.J.R., and C.T.R. developed the mass balance model. A.C.J. and C.M.O. were responsible for data compilation. A.C.J. wrote the manuscript with contributions from C.M.O., A.T.G., C.T.R., T.W.L., and A.D.A. **Competing interests:** The authors declare that they have no competing interests. **Data and materials availability:** All data needed to evaluate the conclusions in the paper are present in the paper and/or the Supplementary Materials.

Submitted 14 April 2021

Accepted 9 August 2021

Published 29 September 2021

10.1126/sciadv.abj0108

Citation: A. C. Johnson, C. M. Ostrander, S. J. Romaniello, C. T. Reinhard, A. T. Greaney, T. W. Lyons, A. D. Anbar, Reconciling evidence of oxidative weathering and atmospheric anoxia on Archean Earth. *Sci. Adv.* **7**, eabj0108 (2021).